UAV Selection in Aerial Integrated Sensing and Communication Networks

Petros S. Bithas
Digital Industry Technologies, National & Kapod. Univ. of Athens,
Psahna, 34400 Evia, Greece
email: pbithas@dind.uoa.gr

George P. Efthymoglou
Digital Systems, University of Piraeus,
Piraeus 18534, Greece
email: gefthymo@unipi.gr

Athanasios G. Kanatas
Digital Systems, University of Piraeus,
Piraeus 18534, Greece
email: kanatas@unipi.gr

Konstantinos Maliatsos
Inf. & Commun. Syst. Eng., University of the Aegean,
Samos, Greece
email: kmaliat@aegean.gr

***Abstract*—The application of integrated sensing and communications (ISACs) technology in air-ground networks, which include unmanned aerial vehicles (UAVs), offers unique opportunities for improving both sensing and communication performances. However, this type of networks are also sensitive to the peculiar characteristics of the aerial communications environment, which include shadowing and scattering caused by man-made structures. This paper investigates an aerial ISAC network and proposes a UAV-selection strategy for improved communication performance. We first derive analytical expressions for the received signal-to-interference ratio for both communication and sensing functions. These expressions are then used to analyze the outage probability of the communication part and the ergodic radar estimation information rate of the sensing part. The presented results reveal the impact of shadowing severity and interference on the system's performance.**

***Index Terms*—Integrated sensing and communications, shadowing, unammaned aerial vehicles (UAVs).**

I. Introduction

Integrated sensing and communication (ISAC) technology has been proposed as an efficient solution that allows wireless communication and radar sensing coexistence in the same system. The research for ISAC technology has recently gained an increased interest in an effort to effectively exploit the same radio and hardware resources for both sensing and communication functions [1]. However, the competition for resources (such as limited power, spectrum, antennas, or other hardware components) between the sensing and communication functions presents a significant challenge that needs to be addressed. It is crucial to identify the key performance boundaries and trade-offs between these functions in ISAC systems subject to resource competition.

In the last few years, various contributions exist that investigate the performance of ISAC systems, e.g., [2]–[6]. In [2], an ISAC system was proposed, in which a micro base station (BS) that can simultaneously conduct target sensing and cooperative communication is assumed, under a non-orthogonal downlink transmission scenario. In this context, various performance metrics such as outage probability (OP), communication rate, and sensing detection probability (DP) were analyzed. In [3], a comparison between sensing-communication coexistence (SCC) and ISAC designs utilizing non-orthogonal downlink transmission and transmit antenna selection was performed. Under the assumption of residual hardware impairments and imperfect successive interference cancellation, the performance of the schemes under consideration was evaluated based on the criteria of exact and asymptotic OPs and the probability of successful target detection. In [4], an air-ground ISAC network was examined, which involves unmanned aerial vehicles (UAVs) and ground terrestrial networks. For this important communication scenario, the system architecture and protocol design were explored for four potential use cases, followed by an analysis of Air-Ground ISAC (AG-ISAC) network characteristics and advantages. In [5], the performance tradeoff within distributed ISAC networks was analytically evaluated based on the tools of stochastic analysis and stochastic geometry. Through these analytical findings, a detailed presentation of the performance boundaries and trade-offs between sensing and communication within a distributed ISAC network was given. In [6], a collaborative ISAC network was investigated that exploits coordinated beamforming techniques. In this framework, the signal-to-interference ratio (SIR) statistics were investigated in order to evaluate the spectral efficiency of the proposed scheme. A common characteristic of the previously presented results is that the shadowing effects have not been taken into account, despite the fact that, in aerial communication networks, the effect of large scale fading is dominant.

Motivated by this observation, in this paper, we consider an aerial-ISAC communication network operating over a generic channel model, in which the impact of large scale fading is investigated. In this type of networks, the radio signals transmitted by a UAV-BS, after having traveled through free space, encounter an urban environment. In this urban setting, the signals experience shadowing and scattering due to man-made structures, resulting in extra loss for the air-to-ground link. Therefore, we consider a UAV-selection strategy that offers improved performance with reduced complexity. For this scheme, we derive exact expressions for the statistics of the received SIR, which are then used to investigate the OP, the DP and the ergodic radar estimation information rate (EREIR). The numerical results depict the impact of the shadowing parameter values and the number of interfering signals on the system's performance.

The remainder of this paper is organized as follows. In

Section II, the system model of the ISAC aerial network and the corresponding channel model are given. In Section III, the analytical framework for obtaining the performance measures for both ISAC operations is presented. Simulation settings are given and numerical results are discussed in Section IV. Finally, conclusions are drawn in Section V.

II. System and Channel Model

We consider an ISAC UAV-assisted communication network, in which one out of L UAVs, which operate as aerial BSs, is selected to communicate with the destination receiver, as depicted in Fig. 1. Moreover, UAVs are also responsible for sensing the surrounding environment in order to identify specific targets. Here, the investigation focuses on the downlink for the communication operation. However, similar results can apply for the uplink performance. The time division principle between sensing and communication operations is assumed, as depicted in Fig. 1. During the sensing phase, each UAV of the network transmits a sensing signal in order to identify the target, while in the communication phase, the selected UAV communicates with the target receiver. However, in both the destination as well as at the UAV radars interfering effects occur due to transmissions and echoes from surrounding UAVs.

A. Channel Model

For the aerial channel model both the effects of small scale fading and shadowing are taken into account. More specifically, Nakagami-m fading is considered, which has been found to provide an excellent fit to the fading conditions observed in UAV-to-ground scenarios [7]. The probability density function (PDF) of the random variable g, that models the Nakagami-m distributed channel gain, is given by [8, eq. (2.20)]

$$f_g(x) = \frac{m^m x^{m-1}}{\Omega^m \Gamma(m)} \exp\left(-\frac{mx}{\Omega}\right), \tag{1}$$

where m is distribution's shaping parameter, related to the severity of the fading, Ω denotes the mean square value, and $\Gamma(\cdot)$ is the gamma function [9, eq. (8.310/1)]. The corresponding CDF expression is given by

$$F_g(x) = \frac{\gamma(m, \frac{mx}{\Omega})}{\Gamma(m)} \tag{2}$$

where $\gamma(\cdot,\cdot)$ denotes the lower incomplete gamma function [9, eq. (8.350/1)].

As far as the shadowing effects are concerned, they appear due to the presence of large scale obstacles between the UAVs and the receiver. These shadowing random fluctuations are modeled by the inverse gamma (IG) distribution with PDF given by [7]

$$f_{s_j}(y) = \frac{\overline{\gamma}_j^{\alpha_j}}{\Gamma(\alpha_j) y^{\alpha_j+1}} \exp\left(-\frac{\overline{\gamma}_j}{y}\right), \tag{3}$$

where $\alpha_j > 1$ is the shaping parameter of the distribution, related to the severity of the shadowing, i.e., lower values of α_j result in lighter shadowing conditions, and $\overline{\gamma}_j$ denotes the scaling parameter. Moreover, the CDF of s_j is given by

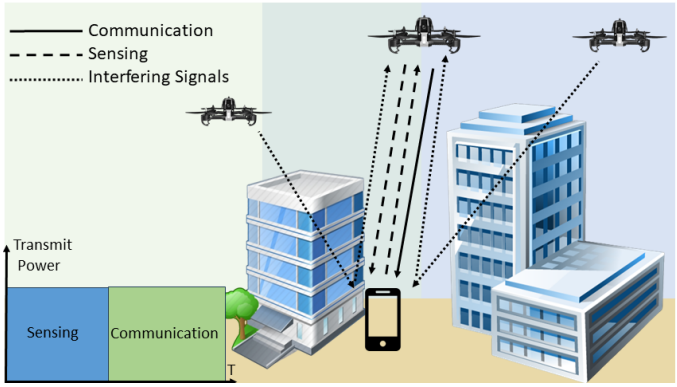

Fig. 1. System model of the considered ISAC scheme.

$$F_{s_j}(y) = \frac{\Gamma(\alpha_j, \frac{\overline{\gamma}_j}{y})}{\Gamma(\alpha_j)}, \tag{4}$$

where $\Gamma(\cdot,\cdot)$ denotes the upper incomplete gamma function [9, eq. (8.350/2)].

As far as the sensing operation is concerned, the received echo signal at a UAV is given by [10]

$$P_{ech} = \frac{p_s G_t G_r \lambda^2 \sigma}{(4\pi)^3 d^{2\nu}}, \tag{5}$$

where p_s denotes the transmitting power of the sensing signal, G_t and G_r denote the transmitting and receiving antenna gains, respectively, λ is the wavelength of the sensing signal, d denotes the distance between the sensing target and the UAV, ν is the path loss factor, and σ is the cross-section of the target. The latter one is a random variable, since it fluctuates from scan to scan, and it follows the Swerling type-1 model, whose PDF is given by [11]

$$f_\sigma(\sigma) = \frac{1}{\bar{\sigma}} \exp\left(-\frac{\sigma}{\bar{\sigma}}\right), \sigma \leq 0 \tag{6}$$

where $\bar{\sigma}$ is the average cross section of the target.

B. Communication Model

As far as the communication part is concerned, it is assumed that the UE is connected to the UAV that is less exposed to shadowing. Moreover, assuming that the noise level is relatively small compared to the aggregate interference, we focus on the interference limited scenario. Under this UAV-selection policy and based on the approach initially proposed in [12], the received SIR is given by

$$\gamma_c = \frac{p_c G_t G_r g s_{\max} d^{-\nu}}{I_c} \tag{7}$$

where p_c denotes the transmit power at the communication phase and $s_{\max} = \max\{s_1, s_2, \cdots, s_L\}$ denotes the maximum shadowing coefficient from the L available UAV-receiver links. Moreover, $I_c = \sum_{i=1}^{M} p_c G_t G_r h_{1,i}^2 d_i^{-\nu}$ denotes the aggregate interference term, with $h_{1,i}$ being the channel gains for the

downlink and d_i is the distance between the i-th, $i = 1, ..., M$ interfering UAV and the receiver.

C. Sensing Model

During the sensing phase, the detection decisions are conducted by using the target echo power P_{ech}. Based on this approach the received SIR at the UAV that senses the target is given by [5]

$$\gamma_s = \frac{P_{ech}}{I_s}, \tag{8}$$

where $I_s = \sum_{i=1}^{M} A_e S h_{1,i}^2 h_{2,i}^2 d_i^{-\nu}$ denotes the aggregate interference term, $h_{1,i}$ and $h_{2,i}$, $i = 1, ..., M$, denote channel gains that follow Nakagami-m fading, $A_e = \frac{G_r \lambda_w^2}{4\pi}$ denotes the effective receiving antenna aperture and $S = \frac{p_s G_t}{4\pi}$ denotes the power density from an interfering UAV.

III. Performance Analysis

For the communication part, the performance of the system under investigation will be investigated using the criteria of the OP and the coverage probability (CP), while for the sensing part the performance metrics that will be employed are the EREIR and the detection probability. The OP is defined as the probability that the instantaneous SIR falls below a predefined threshold $\gamma_{\rm th}$, i.e., $P_{\rm out} = \Pr(\gamma \leq \gamma_{\rm th})$. Moreover, the EREIR is defined as [5]

$$R_B = \frac{\delta}{2T} \log_2 (1 + 2TB_s\gamma_s), \tag{9}$$

where T denotes the pulse duration, B_s denotes the bandwidth, and δ denotes the radar duty cycle. Based on the EREIR, the criterion of DP is defined as follows

$$P_D = \Pr[R_B > \zeta] = \Pr\left[\gamma_s > \frac{2^{\frac{2T\zeta}{\delta}} - 1}{2TB_s}\right], \tag{10}$$

where ζ denotes the detection threshold.

A. Communication Operation

For evaluating the performance of the scheme under consideration, the behavior of the received SIR is statistically evaluated. To this aim, let us define the random variable $Y = \frac{g}{I_c}$. The PDF and CDF of Y are, respectively, given by

$$f_Y(y) = \int_0^\infty x f_g(yx) f_{I_c}(x) dx \tag{11}$$

$$F_Y(y) = \int_0^\infty F_g(yx) f_{I_c}(x) dx. \tag{12}$$

The statistics of I_c are provided in Appendix A. Substituting (1) and (A-3) in (11) and using the definition of the gamma function [9, eq. (8.310)], yields the following closed-form result

$$\begin{aligned} f_Y(y) =& C \sum_{k=0}^{\infty} \frac{\delta_k}{\Gamma(\rho+k)\beta_1^{\rho+k}} \frac{m^m}{\Omega^m \Gamma(m)} y^{m-1} \\ & \times \left(\frac{1}{\beta_1} + \frac{y}{\Omega}\right)^{-k-m-\rho}. \end{aligned} \tag{13}$$

As far as the CDF is concerned, substituting (2) in (12), using [9, eq. (6.455)] and after some mathematical manipulations, yields the following expression

$$\begin{aligned} F_Y(y) =& C \sum_{k=0}^{\infty} \frac{\delta_k}{\Gamma(\rho+k)\beta_1^{\rho+k}} \left(\frac{y}{\Omega}\right)^m \frac{\Gamma(\rho+k+m)}{m\Gamma(m)} \\ & \times {}_2F_1\left(1, \rho+k+m; m+1; \frac{y/\Omega}{y/\Omega + 1/\beta_1}\right) \\ & \times \left(\frac{1}{\beta_1} + \frac{y}{\Omega}\right)^{-k-m-\rho}, \end{aligned} \tag{14}$$

where ${}_2F_1(\cdot)$ denotes the Gauss hypergeometric function [9, eq. (9.100)].

For evaluating the final CDF of γ_c, the statistics of $s_{\max}$ are required, which are provided in Appendix B. Therefore, using (13) and (B-3) in (12), results to

$$\begin{aligned} \mathcal{I} =& \int_0^\infty \left(\frac{y}{x}\right)^{m-1} \left(\frac{1}{\beta_1} + \frac{y}{x\Omega}\right)^{-k-m-\rho} \\ & \times \exp\left(-\frac{\bar{\gamma}M}{x}\right) \left(\frac{\bar{\gamma}}{x}\right)^{\xi} dx \end{aligned} \tag{15}$$

where $\xi = \sum_{i=0}^{\alpha-1} i n_{i+1}$, with n_is denoting integers related to the multiple sums presented below. In order to evaluate this integral and based on [13, eqs. (10) and (11)], the following Meijer G-function representations are used $\left(\frac{1}{\beta_1} + \frac{y}{x\Omega}\right)^{-k-m-\rho} = \left(\frac{1}{\beta_1}\right)^{-k-m-\rho} \frac{1}{\Gamma(k+m+\rho)} G_{1,1}^{1,1}\left(\frac{\beta_1 y}{x\Omega}\middle|\begin{matrix}1-k-m-\rho \\ 0\end{matrix}\right)$, $\exp\left(-\frac{\bar{\gamma}M}{x}\right) = G_{0,1}^{1,0}\left(\frac{\bar{\gamma}M}{x}\middle|\begin{matrix}- \\ 0\end{matrix}\right)$, where $G_{p,q}^{m,n}\left(\cdot\middle|\cdot\right)$ denotes the Meijer G-function. Based on these expressions, using [13, eq. (21)] and after some analysis, results to

$$\begin{aligned} F_{\gamma_c}(x) =& C \sum_{k=0}^{\infty} \sum_{\substack{n_1=0 \\ n_1+n_2+\cdots+n_\alpha=M}}^{M} \sum_{n_2=0}^{M} \cdots \sum_{n_\alpha=0}^{M} \left(\frac{\bar{\gamma}_c}{x}\right)^{\xi} \frac{M!}{n_1! n_2! \cdots n_\alpha!} \\ & \times \delta_k \Gamma(m+k+\rho) \left[\prod_{i=0}^{\alpha-1} \left(\frac{1}{i!}\right)^{n_{i+1}}\right] \\ & \times \left[\frac{\Gamma(m+\xi)\Gamma(k-\xi+\rho)}{\Gamma(m+k+\rho)} \left(\frac{\beta_1}{\Omega}\right)^{-m-\xi}\right. \\ & \times {}_1F_1\left(m+\xi, 1-k+\xi-\rho, \frac{M\bar{\gamma}_c\Omega}{\beta_1 x}\right) \\ & \Gamma(-k+\xi-\rho) \left(\frac{M\bar{\gamma}_c}{x}\right)^{k-\xi+\rho} \left(\frac{\beta_1}{\Omega}\right)^{-m-k-\rho} \\ & \left. \times {}_1F_1\left(m+k+\rho, 1+k-\xi+\rho, \frac{M\bar{\gamma}_c\Omega}{\beta_1 x}\right)\right], \end{aligned} \tag{16}$$

where ${}_1F_1(\cdot)$ denotes the confluent hypergeometric function [9, eq. (9.210/1)], while $\bar{\gamma}_c = \bar{\gamma} p_c G_t G_r d^{-\nu}$.

B. Sensing Operation

For evaluating the sensing performance, the statistical behavior of the received SIR is evaluated. To this aim, let us define the random variable $W = \frac{\sigma}{I_s}$. For evaluating the PDF

TABLE I
SIMULATION PARAMETERS VALUES.

Communication Parameters	**Values**
Wavelength (λ)	0.0833m
Transmit Power (P_c)	15dBm
Tx Antenna Gain (G_t)	10dB
Rx Antenna Gain (G_r)	10dB
Tx-Rx Distance (d)	80m
Path Loss Factor (ν)	2
Number of Interfering Signals (M)	9
Nakagami Parameter (m) for all links	2
Number of UAVs (L)	4
Sensing Parameters	**Values**
Bandwidth (B_s)	20MHz
Pulse Duration (T)	1μsec
Radar Duty Cycle (δ)	0.01

of W, a similar procedure to the one used in the derivation of (13) is adopted, resulting to

$$f_W(y) = C \sum_{k=0}^{\infty} \frac{\delta_k}{\bar{\sigma}\Gamma(\rho+k)\beta_1^{\rho+k}} \left(\frac{1}{\beta_1} + \frac{y}{\bar{\sigma}}\right)^{-k-1-\rho}. \quad (17)$$

The corresponding CDF can be derived as

$$F_W(y) = C \sum_{k=0}^{\infty} \frac{\delta_k}{\Gamma(\rho+k+1)} \left(1 - \left(1 + \frac{\beta_1 y}{\bar{\sigma}}\right)^{-k-1-\rho}\right). \quad (18)$$

Based on (17), the PDF of γ_s can be directly evaluated using a change of variables of the form $W = \gamma_s \frac{(4\pi)^3 d^{2\nu}}{p_s G_t G_r \lambda^2}$, which results to a similar expression to (17), where $\bar{\sigma}$ is substituted with $\bar{\gamma}_\sigma = \bar{\sigma} \frac{p_s G_t G_r \lambda^2}{(4\pi)^3 d^{2\nu}}$. For evaluating the expression for the EREIR, (17) should be substituted in (9). Following such an approach, integrals of the following form appear

$$\mathcal{I}_2 = \int_0^{\infty} \left(\frac{1}{\beta_1} + \frac{x}{\bar{\gamma}_\sigma}\right)^{-k-1-\rho} \log_2(1 + 2TB_s x)\, dx. \quad (19)$$

Using again the Meijer-G function representations for the functions in (19), i.e., using [13, eqs. (10) and (11)] as well as [13, eqs. (21)], yields the following exact expression

$$R_B = \frac{\delta}{2T} C \sum_{k=0}^{\infty} \frac{\delta_k / \ln(2)}{\Gamma(\rho+k)\Gamma(1+k+\rho)} \times G_{3,3}^{2,3}\left(\frac{2B_s T \bar{\gamma}_\sigma}{\beta_1}\middle|_{1,k+\rho,0}^{1,1,0}\right). \quad (20)$$

It is noted that with a small number of terms, i.e., < 20, a satisfactory accuracy is observed in all infinite series expressions derived in this paper.

IV. NUMERICAL RESULTS

In this section, based on the analytical results derived previously, several numerical evaluated results are presented and discussed. If not otherwise stated, in the simulation results, the parameter values depicted in Table I are assumed.

In Fig 2, the OP and DP performances have been evaluated. More specifically, in the left subplot, the OP using UAV selection is plotted as a function of the outage threshold γ_{th}, for various values of the shadowing coefficients $\alpha = \alpha_j$, $j = 1, ..., L$. It is shown that for the same γ_{th}, almost ten times less OP is observed when light shadowing conditions are assumed, i.e., $\alpha = 1$, compared to moderate shadowing, $\alpha = 3$. In the same figure, for comparison purposes, the performance of a scheme without UAV-selection is also presented. It is shown that the performance of the UAV-selection scheme is considerably improved, especially in the case of severe shadowing conditions. In the right subplot of Fig 2, the EREIR is plotted as a function of the transmit power for different distances of the radar target. The plot shows the performance degradation of the sensing operation as the distance increases.

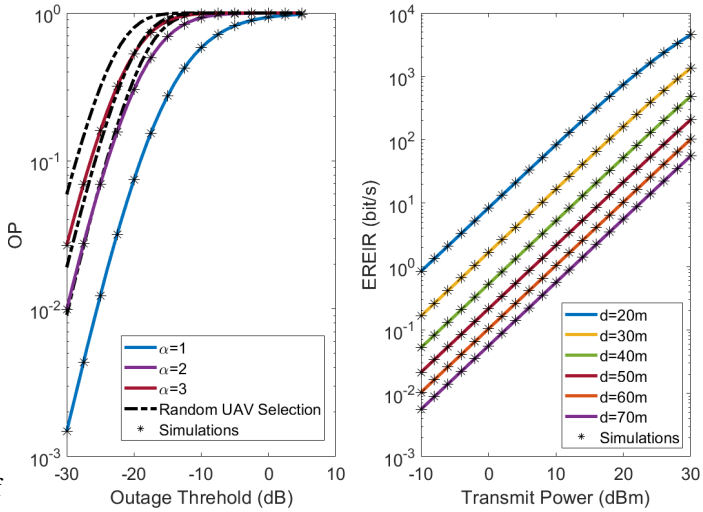

Fig. 2. Communication Function: OP vs the outage threshold. Sensing Function: EREIR vs transmit power.

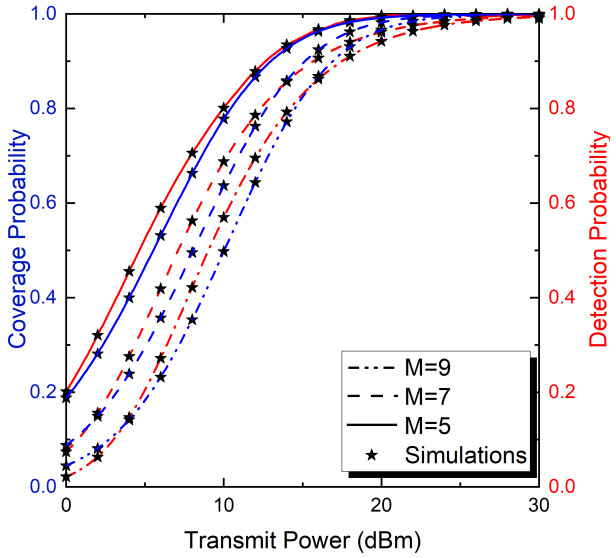

Fig. 3. Coverage Probability and Detection Probability vs transmit power.

In Fig 3, we investigate the effect of aggregate interference by plotting the coverage probability (defined as CP$= 1 - P_{\text{out}}(\gamma_{\text{th}})$ with $\gamma_{\text{th}} = 0dB$) and the DP of the sensing operation as a function of the transmit power, for different

values of the number of interfering signals. It is shown that the number of interfering signals has an important influence on the performance of both operations. Finally, it is noted that in all figures simulations results have been also included, verifying the validity of the presented analysis.

V. Conclusions

In this paper, a new UAV selection strategy is proposed for an aerial ISAC network. To this aim, we presented an analytical framework in order to evaluate the coverage probability of the scheme under consideration and the EREIR of each UAV. The presented results revealed the impact of shadowing and interference on the system's performance. It was shown that the performance of the communication function can be considerably improved using a shadowing based UAV selection policy.

Appendix A
Statistics of the Sum of Gamma RVs

Let us assume that RV I_i is defined as follows

$$I_i = p_c G_t G_r h_{1,i}^2 d_i^{-\nu}. \tag{A-1}$$

Here, RV I_i is approximated by a gamma RV G_i, whose shaping and scaling parameters can be evaluated using the moment matching method, e.g., [14]. Based on this assumption, Y is now represented by a sum of M gamma RVs given as follows

$$I_q = G_1 + G_2 + \cdots + G_M, \tag{A-2}$$

where $q \in \{s, c\}$. Based on [15], the PDF of I_q is given by

$$f_{I_q}(x) = C \sum_{k=0}^{\infty} \frac{\delta_k x^{\rho+k-1}}{\Gamma(\rho+k)\beta_1^{\rho+k}} \exp\left(-\frac{x}{\beta_1}\right), \tag{A-3}$$

where $\beta_i = \frac{\Omega_i}{m_i}$, $\beta_1 = min(\beta_i)$, while

$$C = \prod_{i=1}^{M} \left(\frac{\beta_1}{\beta_i}\right)^{m_i},\ \rho = \sum_{i=1}^{M} m_i,\ \gamma_k = \sum_{i=1}^{M} \frac{m_i}{k}\left(1 - \frac{\beta_1}{\beta_i}\right)^k \tag{A-4}$$

$$\delta_{k+1} = \frac{1}{k+1} \sum_{i=1}^{k+1} i\gamma_i \delta_{k+1-i}, \quad k = 0, 1, 2, \cdots \tag{A-5}$$

with $\delta_0 = 1$.

Appendix B
Statistics of the Maximum of Inverse Gamma RVs

In this appendix, a simplified expression for the CDF of $s_{\max}$ is presented. Assuming independent and identically distributed conditions, i.e., $\alpha_j = \alpha$ and $\bar{\gamma}_j = \bar{\gamma}$, and based on probability laws, the CDF of $s_{\max}$ is given by

$$F_{s_{\max}}(y) = F_s(y)^M = \left[\frac{\Gamma(\alpha, \frac{\bar{\gamma}}{y})}{\Gamma(\alpha)}\right]^M. \tag{B-1}$$

Assuming integer values for the shaping parameters α and using [9, eq. (8.352/2)], (B-1) can be written as

$$F_{s_{\max}}(y) = \exp\left(-\frac{\bar{\gamma}M}{y}\right)\left[\sum_{i=0}^{\alpha-1}\left(\frac{\bar{\gamma}}{y}\right)^i \frac{1}{i!}\right]^M. \tag{B-2}$$

Using the multinomial identity [16, eq. (24.1.2)], yields

$$F_{s_{\max}}(y) = \exp\left(-\frac{\bar{\gamma}M}{y}\right) \sum_{n_1=0}^{M} \sum_{n_2=0}^{M} \cdots \sum_{\substack{n_\alpha=0 \\ n_1+n_2+\cdots+n_\alpha=M}}^{M} \frac{M!}{n_1! n_2! \cdots n_\alpha!} \times \left[\prod_{i=0}^{\alpha-1}\left(\frac{1}{i!}\right)^{n_{i+1}}\right]\left(\frac{\bar{\gamma}}{y}\right)^{\sum_{i=0}^{\alpha-1} i n_{i+1}}. \tag{B-3}$$

Acknowledgement

This work was co-funded by University of Piraeus Research Centre and the EU HORIZON programme under iSEE-6G GA No. 101139291.

References

[1] Z. Xiao and Y. Zeng, "Waveform design and performance analysis for full-duplex integrated sensing and communication," *IEEE J. Sel. Areas Commun.*, vol. 40, no. 6, pp. 1823–1837, 2022.

[2] M. Liu, M. Yang, H. Li, K. Zeng, Z. Zhang, A. Nallanathan, G. Wang, and L. Hanzo, "Performance analysis and power allocation for cooperative ISAC networks," *IEEE Internet Things J.*, vol. 10, no. 7, pp. 6336–6351, 2022.

[3] M. Liu, M. Yang, Z. Zhang, H. Li, F. Liu, A. Nallanathan, and L. Hanzo, "Sensing-communication coexistence vs. integration," *IEEE Trans. Veh. Technol.*, vol. 72, no. 6, pp. 8158–8163, 2023.

[4] Z. Fei, X. Wang, N. Wu, J. Huang, and J. A. Zhang, "Air-ground integrated sensing and communications: Opportunities and challenges," *IEEE Communications Magazine*, vol. 61, no. 5, pp. 55–61, 2023.

[5] X. Li, S. Guo, T. Li, X. Zou, and D. Li, "On the performance trade-off of distributed integrated sensing and communication networks," *IEEE Wirel. Commun. Lett.*, vol. 12, no. 12, pp. 2033–2037, 2023.

[6] K. Meng, C. Masouros, G. Chen, and F. Liu, "BS coordination optimization in integrated sensing and communication: A stochastic geometric view," *arXiv preprint arXiv:2401.04918*, 2024.

[7] P. S. Bithas, V. Nikolaidis, A. G. Kanatas, and G. K. Karagiannidis, "UAV-to-ground communications: Channel modeling and UAV selection," *IEEE Trans. Commun.*, vol. 68, no. 8, pp. 5135–5144, 2020.

[8] M. K. Simon and M.-S. Alouini, *Digital Communication over Fading Channels*, 2nd ed. New York: Wiley, 2005.

[9] I. S. Gradshteyn and I. M. Ryzhik, *Table of Integrals, Series, and Products*, 6th ed. New York: Academic Press, 2000.

[10] P. Ren, A. Munari, and M. Petrova, "Performance tradeoffs of joint radar-communication networks," *IEEE Wirel. Commun. Lett.*, vol. 8, no. 1, pp. 165–168, 2018.

[11] Z. Fang, Z. Wei, X. Chen, H. Wu, and Z. Feng, "Stochastic geometry for automotive radar interference with RCS characteristics," *IEEE Wirel. Commun. Lett.*, vol. 9, no. 11, pp. 1817–1820, 2020.

[12] P. S. Bithas, A. G. Kanatas, and D. W. Matolak, "Exploiting shadowing stationarity for antenna selection in V2V communications," *IEEE Trans. Veh. Technol.*, vol. 68, no. 2, pp. 1607–1615, 2018.

[13] V. S. Adamchik and O. I. Marichev, "The algorithm for calculating integrals of hypergeometric type functions and its realization in REDUCE system," in *Proc. Int. Conf. on Symbolic and Algebraic Computation*, Tokyo, Japan, 1990, pp. 212–224.

[14] P. S. Bithas, G. A. Ropokis, G. K. Karagiannidis, and H. E. Nistazakis, "UAV-assisted communications with RIS: A shadowing-based stochastic analysis," *IEEE Trans. Veh. Technol.*, 2024.

[15] P. G. Moschopoulos, "The distribution of the sum of independent gamma random variables," *Annals of the Institute of Statistical Mathematics*, vol. 37, no. 1, pp. 541–544, 1985.

[16] M. Abramowitz and I. A. Stegun, *Handbook of mathematical functions: with formulas, graphs, and mathematical tables*. Courier Corporation, 1964, vol. 55.